Progress In Electromagnetics Research, Vol. 128, 1–17, 2012

COMPREHENSIVE ANALYSIS OF LENZ EFFECT ON THE ARTIFICIAL HEART VALVES DURING MAGNETIC RESONANCE IMAGING

L. Golestanirad[1,*], E. Dlala[2], G. Wright[1], J. R. Mosig[3], and S. J. Graham[1]

[1]Department of Medical Biophysics, University of Toronto, Toronto, Canada

[2]ANSYS, Inc. Ann Arbor, Michigan, US

[3]Laboratory of Electromagnetics and Acoustics, Ecole Polytechnique Fédérale de Lausanne (EPFL), Lausanne 1015, Switzerland

Abstract—This work presents results of a comprehensive analysis of the Lenz effect due to motion of artificial heart valves during magnetic resonance imaging. The interaction of rotating metallic heart valves with magnetic fields is studied by performing a time-domain analysis of the corresponding electromagnetic problem. We applied the finite element method (FEM) to solve the $T-\Omega$ formulation of Maxwell equations in two cases: first, for metallic disks located in the high intensity homogenous field of the magnet iso-center, and second, disks located in the non-uniform fringe field of the bore entrance. We showed that for valves with full solid disks (such as Starr-Edwards 6500) located in the magnet iso-center, the magnitude of adverse forces can be comparable to the forces applied by the beating heart. However, for rings which consist of multiply connected conductive regions, skin effect and proximity effect counteract, which leads to a diminished magnetic force. Results of this study show that mechanical heart valves with strengthening rings may be considered safe even under ultra-high imaging conditions with field intensities as high as 10 T. However, heart valves with full conducting disks should be considered as a contraindication to MR imaging.

Received 15 March 2012, Accepted 18 April 2012, Scheduled 12 May 2012

* Corresponding author: Laleh Golestanirad (golestan@sri.utoronto.ca).

1. INTRODUCTION

Cardiovascular magnetic resonance (CMR) is a gold standard imaging modality for the evaluation of patients with cardiovascular conditions. The technique is increasingly used for estimation of myocardial structure, wall motion, perfusion and viability. In addition, CMR has inherent safety advantages, particularly, its noninvasive nature and the absence of exposure to ionizing radiation [1, 2]. As a result, a significant increase in the number of magnetic resonance imaging (MRI) scans performed annually has been observed including MRI of patients with cardiovascular implants. Although millions of patients have implanted cardiac devices, MRI was not for many years allowed for these patients because of the potential interference of MRI machines with their devices [3]. It was estimated that at least 200,000 patients with cardiac devices had been denied an MRI scan in 2004 alone [4].

Prosthetic heart valves and annuloplasty rings are commonly composites of different metallic materials such as chromium, cobalt, stainless steel and pyrolytic carbon [5, 6] which when tested, mostly have exhibited measurable but only minor magnetic field interactions due to translational and torsion forces. The magnetic attractive forces on heart valves and annuloplasty rings have been found to be much less than the 7.2-N force exerted by a beating heart [7]. Consequently, the American College of Cardiology Foundation/American Heart Association have considered heart valves and coronary stents to be MR compatible, since they are non-ferromagnetic.

Nevertheless, some concerns have been raised in the past after a theoretical assessment of moving valves with tilting disks or leaflets when considering the Lenz effect. According to the theory, a resistive force may develop in the valve due to its motion in the magnetic field that inhibits the valve from either opening or closing. Although the adverse effects of Lenz forces have not been clinically reported, the theoretical assessment indicated that these forces could reach values up to 100 times greater than those associated to ferromagnetism [8, 9].

This concern seems more rational considering the fast pace toward ultra-high field MR systems, which already use static fields as high as 11.7 T in research on human subjects and 7 T for clinical applications. Despite the need for having a reliable estimation of the significance of Lenz forces on heart valves, theoretical efforts to formulate the problem remain limited. To the authors knowledge, the only quantitative works on this problems are those by Condon and Hadley [8] and Robertson et al. [9]. These works raised an alarm and drew the attention of researchers to a potentially significant source of interaction between passive metallic implants and static magnetic fields which

was overlooked in the conventional approach. However, the results were hindered by an oversimplified formulation of the electromagnetic problem. For example, Condon and Hadley [8] used a simple model based on first order eddy currents to estimate maximum forces applied on heart valves with metal strengthening ring. The results predicted concerning high forces even at relatively low field values (1.5 T), particularly for heart valves in the mitral position. Normal opening and closing pressure differentials are much less in the mitral position than for valves in the aortic position. The model nevertheless, was based on the first order estimation of eddy currents, which did not account for the skin effect: a phenomenon which will be shown to significantly reduce the overall currents and torques.

In this contribution, we describe a comprehensive analysis of the rotational motion of conducting disks in both uniform and non-uniform magnetic field regions of a typical MR scanner. We performed a time-domain analysis of the corresponding electromagnetic problem by applying the finite element method (FEM) to solve the Maxwell equations governing the motion in the presence of magnetic fields. In the case of a uniform magnetic field, in addition to the FEM analysis, analytical formulation has been derived based on the first order estimation of eddy currents. We demonstrated that in the case of a full solid disk, the proposed simplified formulation agrees well with the prediction of the FEM analysis. In contrast, for moving rings consisting of multiple connected conductive regions, the superposition of skin effect and proximity effect leads to significantly less applied magnetic force.

We also analyzed the movement of heart valves in highly non-uniform magnetic fields encountered in the fringe fields at bore entrance of an MRI magnet. This situation might be encountered when the patient undergoes the imaging of the lower limb or knee, and thus is placed in the magnet feet first. The heart valve may then be outside the highly homogeneous volume of the field and will move through regions of rapidly changing flux density during the cardiac cycle. The possibility of adverse interactions in such cases was mentioned but not investigated in previous works.

The outline of this paper is as follows: Section 2 describes the modeling and design of a typical MR magnet using FEM simulations. Section 3 then analyzes the motion of the heart valve in the homogenous field of the magnet iso-center and computes motion-induced forces. It shows that the predictions of the simplified analytical solutions are valid for full solid disks but cannot be extended to rings and strengthening wires, which require a more rigorous method such as the FEM. Finally, in Section 4, the motion of heart valves located

in the fringe field of a typical MRI scanner is analyzed to investigate the effect of field inhomogeneity on the motion of heart valves.

2. MAGNET DESIGN AND MODELING

MRI magnets require the field uniformity better than 10 ppm (part per million) within a spherical imaging volume of diameter 40 to 50 cm and are classified into two classes: shielded and unshielded magnets. In the former case, the stray field may reach more than 100 gauss(G) and it needs a special room for the magnet to protect the electronic equipment from adverse effects. Next generation magnets came with the concept of active shielding where the stray field is less than 4 G (in regions at least 4 m away from the iso-center) either by using ferromagnetic materials [11] or using coaxial coils carrying current in the opposite direction [12]. Different methods are used to design magnets of highly homogeneous field, based on stochastic optimization [20], matrix subset selection [21], inverse approach [22], hybrid numerical methods [23] and methods for permanent magnet design [24].

In this work, we started with the design parameters proposed by Sinha et al. [13] who used blocks of circular loops and optimized the block size to produce desired field uniformity on the axis. Four pairs of coils were used (see Fig. 1) with the direction of current flow counter clockwise in all the three smaller pairs. The current direction in the outermost coil pair was clockwise to model the effect of active shielding. The magnet was symmetric about $z = 0$ plane and each pair of rectangular coil block was determined by four parameters: Z_{jMAX}, Z_{jMIN}, R_{jMAX} and R_{jMIN} where j refers to the block number. These parameters were then optimized to achieve the desired field profile.

We used the Maxwell 3D [14] magneto-static solver which applies FEM to solve the following two equations:

$$\nabla \times \vec{H} = \vec{J} \tag{1}$$

$$\nabla.\vec{B} = 0 \tag{2}$$

The Ansoft FEM solver was set to follow an adaptive iterative process whereby an initial mesh was seeded according to the geometrical details of the structure, with approximately 72000 tetrahedral elements. We set the adaptive solver to refine the mesh for 30% at each iteration and to continue refinement until the difference between two iterative solutions was $< 1\%$. The final number of tetrahedral elements was approximately 122000 cells. The four-coil magnet system was enclosed in a cubic box of 9 m length with the Neumann boundary condition set on its outer faces. Block parameters and current values were initially chosen according to suggestions from [13] and were optimized

using Maxwells embedded Quasi Newton optimizer to mimic the field distribution of a typical 3 T scanner (Discovery MR7502 system) in the vicinity of its bore. The details of optimized geometry is given in Table 1.

Table 1. Details of geometry for actively shielded magnet depicted in Fig. 1. The current density assigned to each terminal coil is set to $J = 7.1 \times 10^8$ [A/m^2].

Coil No.	$R_{\min}$ [cm]	$R_{\max}$ [cm]	$Z_{\min}$ [cm]	$Z_{\max}$ [cm]	Current Density
1	59.98	64.47	9.16	11.26	$+J$
2	61.49	66.19	32.95	37.65	$+J$
3	53.22	58.42	69.07	74.88	$+J$
4	94.69	98.23	68.98	74.98	$-J$

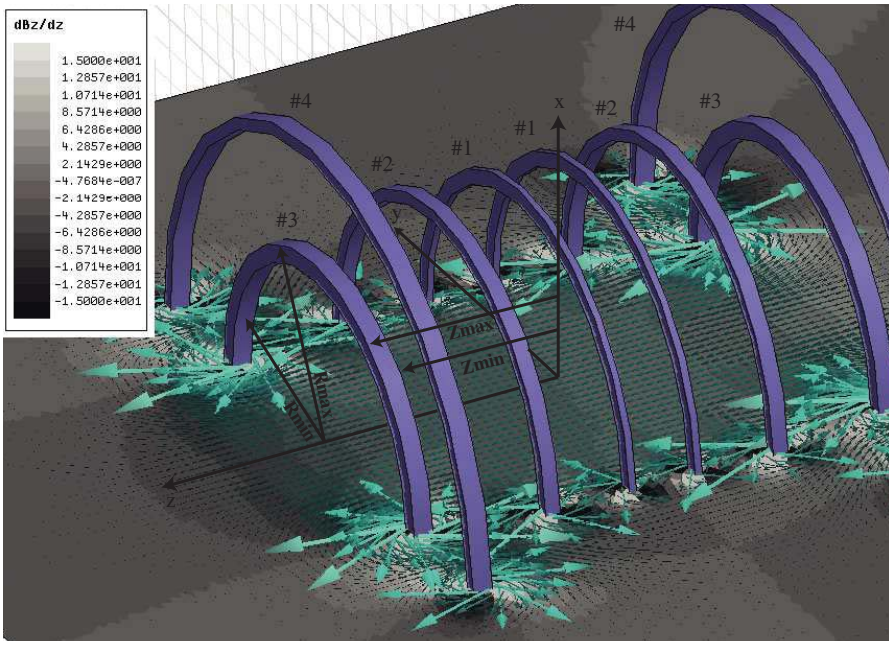

Figure 1. Arrangement for the four pair of coils. Each pair is characterized with a set of parameters Z_{jMAX}, Z_{jMIN}, R_{jMAX} and R_{jMIN} with the current density J flowing clockwise in pairs #1, #2 and #3 and counter clockwise in pair #4. Distribution of magnetic field gradient, dB_z/dz is demonstrated.

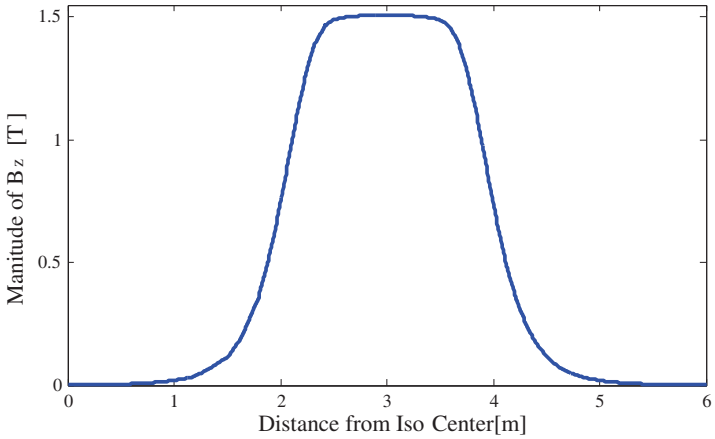

Figure 2. Magnitude of magnetic field along a line passing through magnet iso-center.

Figure 1 also gives the vector representation of the magnetic field over the transverse surface passing through magnet center, overlaid on the distribution of the magnitude of the field gradient, dB_z/dz. It can be observed that the field gradient reaches values as high as 14 T/m in regions close to the bore entrance. These values are in agreement with the reported values[†]. Figure 2 depicts the distribution of the magnitude of B_z along a line passing through magnet iso-center which shows a very high level of uniformity and thus validates the final design. Once the magnet was designed, we performed a time-domain analysis to investigate motion-induced eddy currents and forces imposed on the rotating valve located in two different regions: the highly uniform and high intensity field region in the magnet iso-center and the highly non-uniform region in the bore entrance. For the former case, an analytical formulation is also developed to verify the results of FEM simulations. The details are described in the following sections.

3. HEART VALVE IN THE HOMOGENEOUS MAGNETIC FIELD

There are many types of mechanical valves produced by various manufacturers. In this study we focus on the solid metal disc type and the ring-strengthener type which are more likely to be affected by the Lenz effect. Here, it is important to note that despite the prevalence of

[†] GE Health Care, Discovery MR750 3.0 T Pre-installation Manual, Direction 5500101, Revision 4.0.

non-metallic materials used to construct modern bi and single leaflet mechanical valves, some older single leaflet valves used titanium and Stellite. We also need to consider that older patients are more likely to possess older valves with metal components and, because of age, which weakens the heart muscle, they are likely to be the most at risk.

3.1. First Order Estimation of Motion-Induced Eddy Currents: Analytical Solution

We adopted a unified approach to both solid disks and ring-strengthening valves by analyzing the hollow disk of Figure 3. By doing so, the ring-strengthening valve is the special case when a approaches b ($a \to b$).

Suppose that a thin conducting ring with inner radius of a, outer radius of b and thickness of h is located in a uniform magnetic field B_0, that without lack of generality, is assumed to lie in yz plane and make the angle θ with the normal to the ring surface. If we assume that the ring is rotating around the $\hat{x}$ axis such that θ is a function of time $\theta(t)$, then the magnetic flux ϕ passing through the surface of the ring also varies with time and according to Faradays law of induction, an electromotive force is induced along any closed contour $\partial \sum$ which

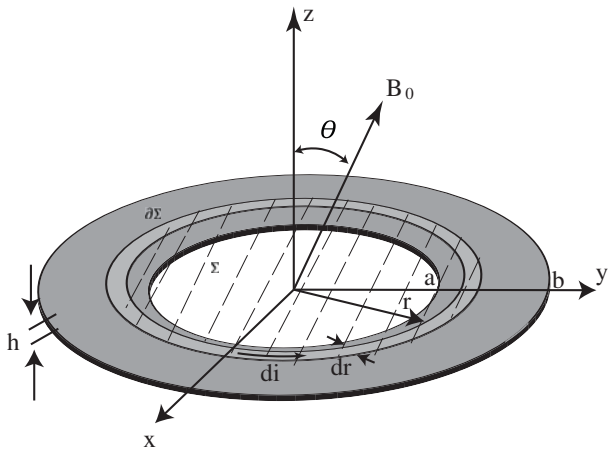

Figure 3. Geometry of a rotating ring with inner radius of a, outer radius of b and thickness of h in a uniform magnetic field. The angle θ between the magnetic field vector and the normal to the ring surface is a function of time as $\theta = \theta(t)$.

encloses the surface $\sum$ in the ring, as depicted in Fig. 3:

$$\oint_{\partial \sum} \vec{E} \cdot d\vec{l} = -\frac{\partial}{\partial t} \int_{\sum} \vec{B} \cdot d\vec{S} \tag{3}$$

We consider the surface of the ring composed of circular elements of radius r and incremental width of dr. To simplify the problem, we only consider the component of electric field $\vec{E}$ which is parallel to the contour $\partial \sum$, as this is the electrical field producing circular currents in the disk. Eq. (3) can be then simplified to give:

$$E = E_\phi = \frac{1}{2} B_0 r \frac{d\theta(t)}{dt} \sin(\theta(t)) \tag{4}$$

The incremental current dI flowing in each elemental circular path can be calculated by multiplying the current density $\vec{J} = \sigma \vec{E}$ by the cross-section of the path hdr:

$$dI = \frac{1}{2} B_0 \sigma r h \frac{d\theta(t)}{dt} \sin(\theta(t)) dr \tag{5}$$

It is important to note that Eq. (5) ignores the skin effect. In other words, the induced current dI is assumed to be only the result of externally changing magnetic flux. According to Maxwell equations, the induced time-varying current itself produces an opposing magnetic field which is the source of secondary eddy-currents. However, in the first order analytic analysis, we ignore the presence of these secondary eddy-currents and proceed with the torque and force computation. The complete treatment of the phenomenon considering all sources of currents will be carried out in Subsection 3.2 using the FEM approach.

The incremental torque imposed over each circular current path that carries current dI can be computed as:

$$d\vec{\tau} = d\vec{\mu} \times \vec{B} \tag{6}$$

where $\vec{\mu}$ is the magnetic moment vector of the differential current loop $\vec{\mu} = dIS\hat{z}$, with S being the surface area enclosed by the current path. Substituting Eq. (5) into Eq. (6) gives the differential torque as:

$$d\tau = d\tau_x = dISB_0 \sin(\theta(t)) = \frac{\pi}{2} B_0^2 \sigma r^3 h \frac{d\theta(t)}{dt} \sin^2(\theta(t)) dr \tag{7}$$

where θ is the angle between normal to the surface of the circle and the external field at each instant of time. Integrating over the whole surface of the ring gives the total torque as:

$$\tau = \frac{\pi}{8} \sigma h \left(b^4 - a^4\right) \frac{d\theta(t)}{dt} \sin^2(\theta(t)) \tag{8}$$

The torque computed in (8) is the result of the superposition of incremental Lorentzs forces applied to each elemental volume of the disk. However, for a ring rotating around one hinged end, we can introduce equivalent force acting on an effective lever arm of length equivalent to the rings diameter $2b$:

$$F = T/2b \tag{9}$$

3.2. Time-domain FEM Analysis of 3D Eddy Currents

To obtain a full description of the phenomenon and account for field inhomogeneities as well as higher order eddy currents, we need to address Maxwells equations directly in their quasi-static form. In order to do this, the designed magnet geometry described in Section 2 design was imported into Maxwell 3D transient solver which applies the FEM to solve the $T-\Omega$ formulation of Maxwell's equations which is a well-developed technique adopted for modeling three-dimensional eddy-current problems [18, 19]. The method is based on introducing a magnetic scalar potential Ω in the whole domain and a current vector potential $\vec{T}$ in the conducting region. More generally, the magnetic field H can be further split into four components [19]:

$$\vec{H} = \vec{H}_s + \vec{T} + \nabla\Omega + \sum \vec{T}_k \tag{10}$$

where $\vec{H}_s$ is the source field due to known total currents or known current densities in either solid conductors or stranded conductors, $\vec{T}_k$ is the source field due to unknown currents in a voltage-driven stranded winding k or solid conductor loop k. Applying Ampere's law, Faraday's law, and Gauss' law for the solenoidality of the flux density yields the differential equations in conducting region as:

$$\nabla \times \left(\frac{1}{\sigma}\nabla \times \vec{T}\right) + \frac{d}{dt}\left(\mu\vec{T} + \mu\nabla\Omega + \sum \mu\vec{T}_k\right) = -\frac{d}{dt}(\mu H_s) \tag{11}$$

$$\nabla.\left(\mu\vec{T} + \mu\nabla\Omega + \sum \mu\vec{T}_k\right) = -\nabla\cdot(\mu H_s) \tag{12}$$

where μ is the permeability. In non-conducting regions, the field equation reduces to:

$$\nabla.\left(\mu\nabla\Omega + \sum \mu\vec{T}_k\right) = -\nabla.(\mu H_s) \tag{13}$$

The problem region is then discretized into tetrahedral elements and the standard FEM approach can be applied to solve the equations.

Maxwell 3D allows for both translational and rotational motion and automatically calculates motion-induced eddy currents. The details of FEM implementation scheme can be found in [15].

To investigate the rotational motion of heart valves in the uniform magnetic field (e.g., the field in the magnet iso-center), we studied three cases of: a) the full solid disk with the radius of 20 mm, b) the ring with the outer radius of 20 mm and the inner radius of 10 mm and c) the ring with the outer radius of 20 mm and the inner radius of 18 mm. In all three cases, the disk thickness was 2 mm and the disk was located at the center of the magnet bore of Fig. 1. The mesh size was chosen such that doubling the number of element would lead to less than 1% change in the final results.

Single leaflet tilting disc valves are commonly restricted to opening by 60° to 70° [16] and others may open up to 75° [17]. The opening should take place in less than 50 ms [16] if the artificial valve is to mimic the function of a normal heart valve. The angular frequency of the rotation was set to 50π which corresponds to 90° opening in 10 ms as the worst case scenario. The total time allowed for the motion was set to 10 ms with time steps of $dt = 0.025$ ms.

3.3. Numerical Results

Figure 4 shows the distribution of eddy currents on the surface and outer region of the rotating disk placed in the homogeneous magnetic field of the magnet iso-center. The computed torque is demonstrated in Fig. 5 and is compared with the results of the analytical formulation. It can be observed that, for the full disk, the results of the 3D FEM analysis of eddy currents agree closely with the prediction of the simplified formulation given in Eq. (8), which neglects the skin effect. This was expected considering that for the full disk, the skin effect, which causes currents to move toward the conductor edges, acts in accordance with currents calculated by Eq. (5), which predicts the maximum current to flow at the outer edge of the disk. However, one expects that in the case of a hollow conductor, e.g., a disk with a circular hole in the middle, the skin effect does not act in accordance with the computed currents of Eq. (8) anymore. In this case, the second order eddy currents, which are the result of the time varying magnetic field produced by first order eddy currents represented in Eq. (5), will result in a current profile that reaches its maximum at both the outer and inner edges. This is confirmed by performing the 3D FEM analysis of eddy currents as depicted in Fig. 4(d). It can be observed that in this case, the direction of currents on the inner edge is opposite of those on the outer edge, an effect that leads to a total torque that is considerably smaller in comparison to the one computed from (8). Fig. 5 shows the comparison between the torque predicted by Eq. (8) and the computed torque solving the modified formulation by FEM (dashed lines). The effect is even more pronounced in the case

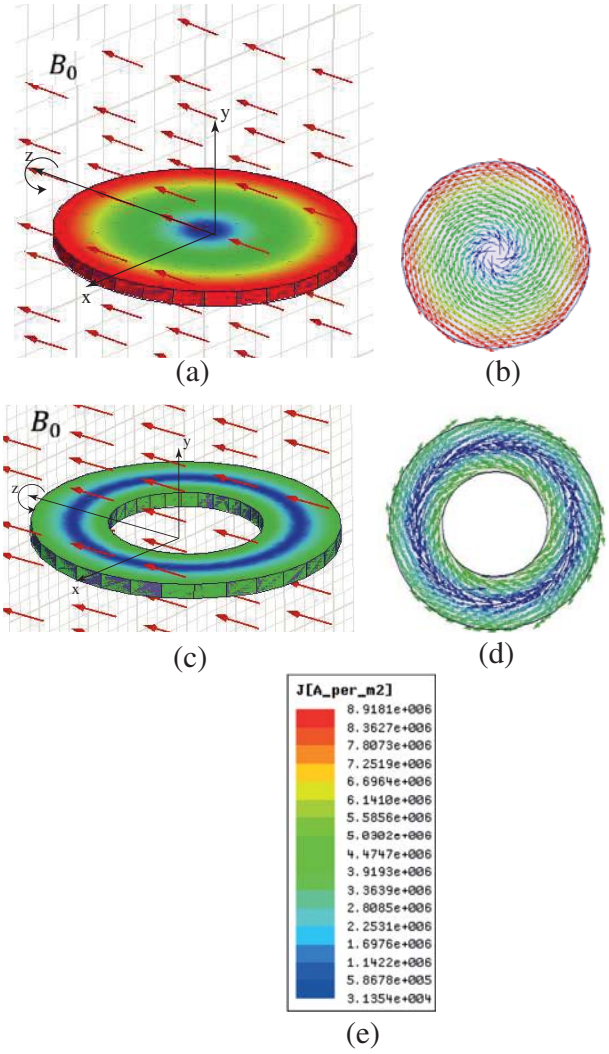

Figure 4. (a) and (b): Magnitude and vector plot of current density distribution on the surface of a full disk rotating in the uniform magnetic field. The disk is made of titanium with the radius of $b = 20\,\text{mm}$ and height of $h = 2\,\text{mm}$. (c) and (d): Magnitude and vector plot of current density distribution on the surface of a ring rotating in the uniform magnetic field. The ring is made of titanium with the outer radius of $b = 20\,\text{mm}$, inner radius of $a = 10\,\text{mm}$ and height of $h = 2\,\text{mm}$.

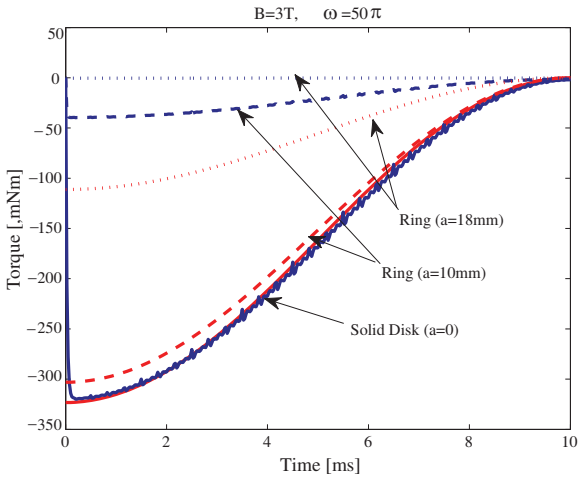

Figure 5. Comparison between the evaluated torque as formulated in Eq. (8) (red lines) and the computed torque applying a 3D FEM analysis (blue lines) for the full disk (solid lines), the ring with inner radius of 10 mm (dashed lines) and the wire-like ring with inner radius of $a = 18$ mm (dotted line).

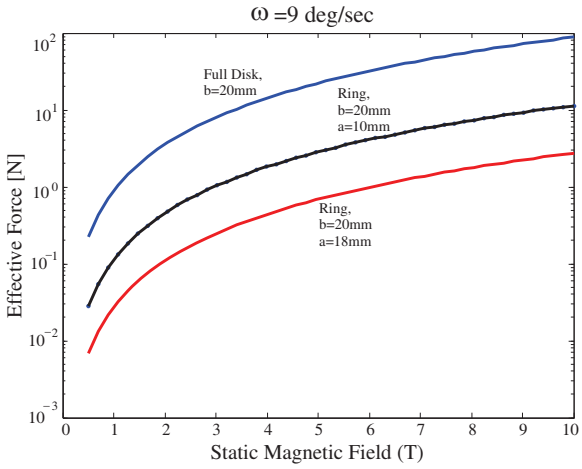

Figure 6. Effective force ($F = T/2b$) applied over the valve as a function of magnetic field for a) full disk, b) ring with the inner diameter half of the outer diameter, and c) wire-like ring. For all cases the valve is opening with speed of 9 degree per second which corresponds to the worst case scenario.

of a wire-like ring, modeled with $a = 18\,\text{mm}$ (corresponding to a wire with cross-section of) where the eddy effect decreases the torque to values as small as 0.1 mN.m that is almost three orders of magnitude smaller than the predictions of Eq. (8).

Figure 6 compares the results of FEM analysis of effective forces imposed over the operating valves for three cases: 1) a full disk, 2) a ring with $a = 10\,\text{mm}$ and 3) the wire ring with $a = 18\,\text{mm}$. In all cases, the valve is opening with the speed of 9 degrees per second, which is considered to be the upper limit.

4. HEART VALVE IN THE FRINGE FIELD OF MRI MAGNET

To study the effect of field inhomogeneity on the motion of a heart valve we analyzed the motion of heart valve located in the fringe field of the magnet. As can be observed from Fig. 1, static field gradients reach values up to 14 T/m in the central region of bore entrance and up to 50 T/m near the coil body. These high gradient regions near the coil body are reported to be inaccessible by the patient in the particular system we have modeled. However, new generation of wide bore scanners (Optima MR460w, 3 T HDx and Signa3.0 T series, for example) produce field products of the same level in areas accessible to patients.

Despite the high values of field gradients, the percent change of magnetic field over the surface due to this spatial inhomogeneity remains negligible. Even if we assume that the heart valve is located at a position where the field gradient reaches the value of 50 T/m, the percentage of field change over the surface of a 40 mm diameter disk is only 500 G which is negligible compared to the rate of change of magnetic field due to the rotational motion of disk. To verify this, we situated the disk in the position in which field gradient reached its highest value at 50 T/m and computed the torque by running the FEM simulation with the same motion parameters as described in Subsection 3.2. The magnitude of magnetic field at this location was 1.8T0.1. The computed torque and consequently, computed forces did not show any noticeable difference from the graphs depicted in Fig. 6 for $T = 1.8\,\text{T}$.

5. DISCUSSION AND CONCLUSION

Mechanical heart valves with metallic components are currently considered MRI compatible because of the absence of ferromagnetic material in their composition. However, concerns have been recently

raised hypothesizing the potential adverse effects of Lenz forces induced by valve motion. The concern seems even more rational considering the fast advancements toward ultra-high field imaging systems which already use field intensities up to 11.7 T. Consequently, a reliable estimation of magnitude of these forces is needed to establish safe and yet not unnecessarily restrictive safety guidelines.

This work presented a rigorous investigation of the Lenz effect on the artificial heart valves during magnetic resonance imaging. In Subsection 3.1, we derived analytical solutions based on the first order estimation of eddy currents. The predictions of the analytical solution were compared with the results of the full-wave analysis for both solid disk and the doubly connected conducting ring. We demonstrated that in the latter case, the formation of higher order eddy currents, which lead to the well-known skin effect phenomenon, reduces the total torque and hence, the effective force applied over the ring surface. However, in all cases, the magnitude of the adverse force increases in proportion to the square of magnetic field. It can be observed from Figure 6 that for the solid disk, the magnitude of Lenz force reaches values as high as 100 N for the magnetic field of 10 T. However, for the wire-like ring, this value remains below 2 N in the whole range of magnetic fields.

We also investigated the effect of high spatial inhomogeneity of magnetic fields at the bore entrance of typical MR scanners. There have been concerns about the situations where the patient undergoes the MRI of lower limb and so enters the scanner feet first. In this case, the heart valve is positioned in the fringe field of the magnet, which is known to be highly inhomogeneous. The spatial distribution of magnetic field is investigated by modeling the full actively shielded magnet. The result of our modeling showed that the percentage of change of magnetic field over the valve surface is negligible compared to the rate of change of magnetic flux due to the rotational motion of the valve. In other words, the worst case estimation of Lenz effect due to operation of heart valves corresponds to the motion of heart valve in the homogeneous high intensity field of magnet iso-center.

In this work, we only investigated the effect of static magnetic. There are other sources of electromagnetic interaction between the MR scanner and metallic objects, such as switching gradients and the RF excitation pulse. However, these sources have a negligible effect on the rotation of heart valves. For example, the amplitude of a 1 ms RF pulse required for a 90° flip angle is only 5.9 μT and the typical magnitude of spatial gradients is in the order of few millitesla (mT). Therefore, these fields do not produce a significant Lorentz force.

In summary, the result of this study shows that mechanical heart valves with strengthening rings may be considered safe even under

ultra-high imaging conditions with field intensities as high as 10 T. This conclusion is based on the fact that the magnitude of Lenz forces due to the valve rotational motion in this case is less than typical forces of a beating heart which is 7.2 N. However, heart valves such as Starr- Edwards 6500 which have solid metallic disk are subject to high adverse forces during MRI even at typical clinical field intensities. For example, the resistive force applied over the surface of a valve with titanium metallic disk at 4 T is approximately 14 N. Considering the surface of the valve, which is 12.6 cm^2, this force is applying a pressure of 83 mmHg over the valves disk. If the valve is located in mitral position, it should open and close under a pressure difference of only a few mmHg (less than 4 mmHg) between the relaxing left ventricle and the left atrium. High resistive pressures as the one computed here, could severely hinder the normal operation of the heart valve and thus, heart valves with full conducting disks should be considered as contraindication to MR imaging.

ACKNOWLEDGMENT

This work was partially supported by a research grant from Swiss National Science Foundation (grant PBELP2-135868).

REFERENCES

1. Pennell, D., U. Sechtem, C. Higgins, W. Manning, G. Pohost, F. Rademakers, A. van Rossum, L. Shaw, and E. Yucel, "Clinical indications for cardiovascular magnetic resonance (CMR): Consensus panel report," *J. Cardiovasc Magn. Reson.*, Vol. 6, No. 4, 727–765, 2004.
2. Mavrogeni, S., F. Rademakers, and D. Cokkinos, "Clinical application of cardiovascular magnetic resonance," *Hellenic J. Cardiol.*, Vol. 45, 401–405, 2004.
3. Roguin, A. and D. Goldsher, "Magnetic resonance imaging and implantable cardiac electronic devices: It's not what we can do, it's what we should do," *Isr. Med. Assoc. J.*, Vol. 12, No. 7, 436–438, 2008.
4. Kalin, R. and M. Stanton, "Current clinical issues for MRI scanning of pacemaker and defibrillator patients," *Pacing Clin. Electrophysiol.*, Vol. 28, 326–328, 2005.
5. Shellock, F. and S. Morisoli, "Ex vivo evaluation of ferromagnetism, heating, and artifacts produced by heart valve

prostheses exposed to a 1.5 T MR system," *J. Magn. Reson. Imaging*, Vol. 4, 756–758, 1994.

6. Edwards, M., K. Taylor, and F. Shellock, "Prosthetic heart valves: Evaluation of magnetic field interactions, heating and artifacts at 1.5 T," *J. Magn. Reson. Imaging*, Vol. 12, 363–369, 2000.
7. Soulen, R., T. Budinger, and C. Higgins, "Magnetic resonance imaging of prosthetic heart valves," *Radiology*, Vol. 154, 705–707, 1985.
8. Condon, B. and D. Hadley, "Potential MR hazard to patients with metallic heart valves: The lenz effect," *J. Magn. Reson. Imaging*, Vol. 12, 171–176, 2000.
9. Robertson, N. M., M. Diaz-Gomez, and B. Condon, "Estimation of torque on mechanical heart valves due to magnetic resonance imaging including an estimation of the significance of the lenz effect using a computational model," *Phys. Med. Biol.*, Vol. 45, 3793–3807, 2000.
10. Garrett, M. W., "Thick cylindrical coil systems for strong magnetic fields with field or gradient homogeneities of the 6th to 20th order," *Journal of Applied Physics*, Vol. 38, No. 6, 2563–2586, 1967.
11. Zhao, H. and S. Crozier, "A design method for superconducting MRI magnets with ferromagnetic material," *Meas. Sci. Technol.*, Vol. 13, 2047, 2002.
12. Kalafala, A. K. and S. Crozier,, "Optimized configurations for actively shielded magnetic resonance imaging magnets," *IEEE Tran. Magn.*, Vol. 27, No. 2, 1696–1699, 1991.
13. Sinha, G., R. Sundararaman, and G. Singh, "Design concepts of optimized MRI magnet," *IEEE Tran. Magn.*, Vol. 44, No. 10, 2351–2360, 2008.
14. Ansys Product Suit., "Maxwell 3D," http://www.ansoft.com/pro-ducts/em/maxwell/, 2011.
15. Henneron, T., Y. L. Menach, F. Piriou, O. Moreau, S. Clnet, J. Ducreux, J. Vrit, J. Villeneuve, and E. Nationale,, "Source field computation in NDT applications," *IEEE Tran. Magn.*, Vol. 43, No. 4, 1785–1788, 2007.
16. Lynch, W., "Implants," *Van Vostrand Reinhold*, 48–94, New York, 1982.
17. Chandran, K., B. Khalighi, and C.-J. Chen,, "Experimental study of physiological pulsatile flow past valve prostheses in a modeof of human aorta-II. Tilting disc valves and the effect of orientation," *Journal of Biomechanics*, Vol. 18, No. 10, 773–780, 1985.

18. Ren, Z., "T-omega formulation for eddy-current problems in multiply connected regions," *IEEE Tran. Magn.*, Vol. 38, No. 2, 557–560, 2002.
19. Zhou, P., W. N. Fu, D. Lin, D. Stanton, and Z. J. Cendes, "Numerical modeling of magnetic devices," *IEEE Tran. Magn.*, Vol. 40, No. 4, 1803–1809, 2004.
20. Crozier, S., "Compact MRI magnet design by stochastic optimization," *J. Magn. Reson.*, Vol. 127, 233–237, 1997.
21. Morgan, P. N., S. M. Conolly, and A. Macovski, "Resistive homogeneous MRI magnet design by matrix subset selection," *Magn. Reson. Med.*, Vol. 41, No. 6, 1221–1229, 1999.
22. Thompson, M. R., R. W. Brown, and V. C. Srivastava, "An inverse approach to the design of MRI main magnets," *IEEE Tran. Magn.*, Vol. 30, No. 1, 108–112, 1994.
23. Zhao, H., S. Crozier, and D. M. Doddrell, "Asymmetric MRI magnet design using a hybrid numerical method," *J Magn. Reson.*, Vol. 141, No. 2, 340–346, 1999.
24. Ravaud, R. and G. Lemarquand, "Magnetic field in MRI yokeless devices: Analytical approach," *Progress In Electromagnetics Research*, Vol. 94, No. 2, 327–341, 2009.